Discover Applied Sciences

Research

Predicting the state of charge of lithium ion battery in e-vehicles using Box-Jenkins combined artificial neural network model

Glarida Amala Louis[1] · **Siddharth Sampathkumar**[2]

Received: 25 July 2024 / Accepted: 12 December 2024
Published online: 10 February 2025

Abstract
This study presented a novel hybrid model for predicting the state of charge (SoC) of lithium-ion batteries in electric vehicles that combines Box-Jenkins approach with artificial neural networks (ANN). Unlike existing approaches that use either linear or nonlinear models, the suggested method mixes the linear Auto-Regressive Moving Average (ARMA) model with a nonlinear Multi-Layer Perceptron (MLP) network. This integration explores the inherent non-stationarity in SoC data by using the Battery Performance Index (BPI), which normalises SoC for improved time-series analysis. The hybrid model outperformed conventional models, with a R^2 of 0.947. Furthermore, it exploited four critical battery parameters—charge rate, voltage, depth of discharge, and energy density—to provide a more precise SoC prediction than previous techniques. The results demonstrate the hybrid model's stability and capacity to capture complicated battery dynamics, establishing it as a significant step forward in SoC estimate for electric vehicles.

Article Highlights

1. The hybrid model combining neural networks and Auto-Regressive Moving Average, improves battery charge predictions.
2. Charge Rate, Voltage, Depth of Discharge, and Energy Density are important considerations in making accurate predictions.
3. The model surpassed established approaches, improving electric car battery efficiency and accuracy.

Keywords State of charge · Lithium ion batteries · e-vehicles · Box-Jenkins · Artificial neural network

1 Introduction

1.1 Motivation and background

The widespread use of Electric Vehicles (EVs), including Plug-in Hybrid Electric vehicles (PHEVs), Hybrid Electric Vehicles (HEVs), and Battery Electric Vehicles (BEVs), has boosted demand for efficient battery technology. According to recent studies [1], lithium-ion (Li-ion) batteries have emerged as the preferable energy source for EVs due to its high energy

✉ Siddharth Sampathkumar, sksmsiddharth1@yahoo.in; Glarida Amala Louis, glaridaamala.eee@mamcet.com | [1]Department of Electrical and Electronics Engineering, M A M College of Engineering And Technology, Trichy-Chennai Trunk Road, Siruganur, Tiruchirapalli 621105, India. [2]Department of Mechanical Engineering, PSN College of Engineering and Technology, Melathediyoor, Tirunelveli 627152, India.

density, long cycle life, and higher charge–discharge efficiency. Despite these advantages, accurate State of Charge (SoC) estimate remains a major challenge, with direct implications for EV range, battery longevity, and performance [2]. Lithium-ion batteries have various advantages over lead-acid batteries, including increased energy density, longer cycle life, and lower maintenance requirements. Li-ion batteries have superior charging and discharging properties. These advantages make lithium-ion batteries a more efficient option for electric vehicles than standard lead-acid batteries.

Li-ion batteries are sensitive to temperature changes, overcharging, and over-discharging, which can dramatically reduce their performance over time [3]. To overcome these problems, current research has looked into advanced data-driven approaches like Artificial Neural Networks (ANNs) that can forecast critical battery metrics, including SoC, with greater accuracy [4]. Manoharan et al. (2023) and Kamali & Lim (2023) found that ANN models can accurately estimate SoC under dynamic conditions [5, 6]. However, the hybridization of traditional linear models such as Auto-Regressive Moving Average (ARMA) with ANN has received less attention, resulting in a gap in the development of more robust prediction models.

1.2 Relevant literature

ANNs are driving recent advances in lithium-ion battery management and performance optimization in EVs. Nouri et al. (2024) used an Artificial Neural Networks with Particle Swarm Optimization (ANN-PSO) algorithm to optimize vehicle-to-grid systems, resulting in improved Battery Efficiency (BE) and energy management [7]. Afzal et al. (2023) suggested a new battery management system using ANN-based adaptive droop control to improve load balance and Overall Battery Performance (OBP) [8]. Adedeji and Kabir (2023) created a feed-forward deep neural network for forecasting SoC, which outperformed existing methods [9]. Mehmandoosti and Kowsary (2023) used ANN-driven multi-objective optimization for battery cooling, emphasizing the importance of thermal control in battery efficiency [10]. Olabi et al. (2024) discussed present capabilities and future research needs for ANN-based prognosis and assessment of Li-ion battery conditions [11]. In Çolak's (2023) study, machine learning models were used to analyze the effect of road gradient and coolant flow on battery components [12]. The findings indicate improvements to system design and efficiency. Kurucan et al. (2024) investigated the use of ANNs in battery management systems, noting improvements in computing efficiency and learning speed [13]. Naresh et al. (2024) addressed predictive machine learning strategies for improving battery performance while addressing real-world issues [14].

Wei et al. (2024) suggested a robust approach for assessing the state of charge in $LiFePO_4$ batteries utilising a Sage-Husa adaptive Kalman filter paired with a dynamic neural network for increased accuracy[15]. Shrivastava et al. (2023) examined advances in Li-ion battery state estimation methods, focusing on gains in EV efficiency [16]. Oyucu et al. (2024) conducted a comparative review of machine learning algorithms for battery performance prediction, with a focus on reliability and efficiency [17]. Badran and Toha (2024) addressed concerns and obstacles in AI battery management, suggesting ways to improve stability and efficiency [18]. Hong et al. (2023) created self-attention mechanism networks for thermal fault detection, which improves battery safety and durability [19]. Scarpelli et al. (2023) used ANN techniques for improving SoC of Lithium Iron Phosphate (LIP) batteries [20]. Lipu et al. (2023) investigated AI techniques to battery management, highlighting future research prospects for improving battery performance [21]. These researches collectively demonstrate the significant improvements in battery management and prediction technologies, fuelled by advanced ANN models and machine learning approaches, which are critical for optimizing the performance and dependability of Li-ion batteries in EVs.

1.3 Contributions and organization

The study contribution described numerous significant advances and modifications in the field of Li-ion battery management and condition estimation for electric cars. The study sought to address the difficulties involved with predicting the State of Charge (SoC) and State of Health (SoH) of Li-ion batteries by combining diverse approaches and technologies.

The study relied on prior research, which had highlighted the need of correct SoC and SoH estimation in enhancing the efficiency and performance of EVs. Earlier studies used ANNs to predict these parameters, demonstrating their usefulness in a variety of settings. Manoharan et al. (2023) used Parallel Artificial Neural Network (PANN) to improve SoC estimates, whereas Kamali and Lim (2023) focused on enhancing the accuracy and resilience of SoC predictions using dynamic analysis [6]. Other studies, such as Wang et al. (2023), used artificial neural networks to anticipate temperature, emphasizing the importance of thermal management in battery performance [22].

The study's innovation lay in its innovative combination of the Box-Jenkins time-series forecasting model with a combined ANN technique for predicting SoC in Li-ion batteries used in EVs. This technology progressed above existing strategies by overcoming restrictions noted in previous research. Previous studies, such as those by Manoharan et al. (2023) [5] and Kamali and Lim (2023) [6], used ANNs to enhance SoC estimation, but their models struggled with dynamic situations and external influences. Similarly, Wang et al. (2023) [22] concentrated on temperature prediction without combining it with SoC predictions. The requirement for improved accuracy and dependability in electric vehicle applications drove the decision to use SoC prediction rather than estimation. Prediction provides proactive insights into battery performance, allowing for more effective energy management decisions. This strategy reduces uncertainty and adjusts to changing operational conditions, resulting in increased lithium-ion battery efficiency and lifespan. Finally, precise SoC prediction promotes developments in electric car technology and improves user experience by optimizing performance.

By combining Box-Jenkins and ANN, this study leveraged the strengths of temporal pattern recognition and nonlinear data handling, with the goal of improving the accuracy and resilience of SoC forecasts. This technique addressed gaps in the literature and provided a novel framework for more precise SoC estimates, which are critical for optimizing battery management systems and improving EV performance.

The main objective of this research was to create a novel method for forecasting the SoC of Li-ion batteries in EVs. This was accomplished by combining the Box-Jenkins time-series forecasting model and ANN. The goal was to improve the accuracy and reliability of SoC predictions, solve limits identified in prior research, and provide a more robust tool for battery management in electric vehicles.

The current study builds on previous advances by introducing a Box-Jenkins mixed ANN model for predicting the SoC of Li-ion batteries. This model attempted to combine the advantages of classic time-series forecasting approaches with the adaptive capabilities of ANNs in order to offer more accurate and trustworthy predictions. The study also attempted to fill existing gaps in the literature about the estimation of SoC in Li-ion batteries used in electric vehicles, which had received less attention.

2 Materials and methods

2.1 E-vehicle lithium ion battery parameters

The commonly used lithium ion batteries in all-electric, plug-in hybrid electric, and hybrid electric vehicles (PHEVs) are the ones taken into consideration in this study. Generally, e-vehicles produced by Garura Electric Scooters, Exo Dynamic Power Vehicles, Srivaru Motors, Ozotec Automobiles, etc., employ these portable batteries. This paper assesses the crucial characteristics of lithium-ion battery of electric vehicles. It introduces a combined method for the prediction of Battery SoC. Battery Capacity (BC), which indicates the total stored energy and is measured in ampere-hours (Ah) or kilowatt-hours (kWh), is one of the key factors that have been found to affect the SoC of electric vehicles. Battery voltage (BV), expressed as volts (V), represents the difference in electric potential. Energy density (ED) measures energy per unit weight or volume (Wh/kg or Wh/L). The power delivery rate in relation to weight or volume is indicated by the power density (PD) (W/kg or W/L). Before capacity decline, charge–discharge cycles are represented by Cycle Life (CL). The charging or discharging speed of batteries is indicated by the charge rate (C_{rate}) [23]. Instead of entire cycles, the partial charging and discharging characteristics were analyzed. While a full charge–discharge cycle determines the battery's state of health (SOH), this study used 300 samples with various profiles. The data most likely reflected parts of distinct charge and discharge cycles rather than whole cycles, with an emphasis on capturing real-world usage scenarios. This approach enabled the model to effectively manage partial cycles, which is consistent with practical battery usage, where entire cycles do not always occur sequentially. The battery's capacity was calculated by measuring the charge throughput during partial charging and draining cycles. The overall capacity was calculated by totaling the charge added during charging and subtracting it during discharging.

Measured in cycles, depth of discharge (DoD) indicates the proportion of capacity used. Temperature range (T_{range}) represents ideal working temperatures, which are essential for identifying efficiency. The loss of charge during inactivity is indicated by the self-discharge rate (SDR). Internal resistance (IR) reduces efficiency by obstructing the flow of current [24]. Secure operations of the batteries are ensured by safety features (SF). Cost (C) includes the cost of manufacturing. Battery Efficiency (BE) measures how well a battery charges and discharges while accounting for losses. Performance and efficiency of batteries are influenced by Internal Heat Generation (IHG) [25].

Battery temperature is regulated by thermal management (TM). Charging and discharging efficiency are improved by voltage efficiency (VE). Based on discharge rate, Peukert's Law Coefficient (PLC) affects the battery capacity. Power production is affected by Voltage Sag (VS). The accuracy of charge release is measured by Coulombic Efficiency (CE) [26]. Space use is optimized by Packing Efficiency (PE). Accurate SoC measurements are essential for best performance. For uniform cell ageing, Balancing Efficiency (BLE) is required. Energy Recovery (ER) raises efficiency levels of batteries. Electrochemical processes of batteries are influenced by Chemical Efficiency (CE) [27].

The percentage of electrical power that is stored or available on board in an electric vehicle is referred to as the battery's SoC). This is expressed as the battery's current remaining capacity divided by its current rated capacity, often known as its maximum current capacity. The equation for calculating SoC is shown in Eq. 1 [28].

$$SOC = \frac{I_a}{I_b} \times 100\% \tag{1}$$

In Eq. 1, battery's available current and maximum current are indicated as I_a & I_b, respectively. The formula for determining battery capacity (BC) is shown in Eq. 2 [28].

$$BC = V \times A_r \tag{2}$$

The battery's rated ampere-hour (A_r) and battery voltage (V), are represented in the Eq. 2, above. The following formula (Eq. 3) is used for computing the Self Discharge Rate (SDR) [29].

$$SDR = \frac{C_{RT} - C_I}{C_I} \times \frac{1}{T} \times 100 \tag{3}$$

In the above Eq. 3, the battery's residual capacity is indicated as C_{RT}, initial battery capacity is indicated as C_I, and time period is denoted as T. A total of 300 data samples were taken into consideration for SoC prediction. For assessment, the manufacturer's specifications and the maintenance engineers' actual data record (record sheet) were obtained. The data record was typically documented in working days, ignoring holidays. The data was gathered for a total of 300 individual days because the replacement guarantee for electric vehicle batteries is typically one year. To assess the mean time between failures, the interval between repairs was noted. The battery efficiency for the gathered data was computed. This study used checklists and service sheets as secondary data and manufacturer and maintenance technician questionnaires as primary data.

Following analysis of the gathered data, Battery Effectiveness Index (BEI) of 0 to 1 was determined. It was evaluated using the following parameters: Energy Recovery (ER), Internal Heat Generation (IHG), Packing Efficiency (PE), Voltage Sag (VS), Safety Feature (SF) Index, Internal Resistance (IR), Cost (C), Thermal Management (TM) Index, Coulombic Efficiency (CE), and Balancing Efficiency (BLE). The Temperature Range (T_{range}), Cycle Life (CL), Power Density (PD), Battery Capacity (BC), Battery Efficiency (BE), Energy Density (ED), Depth of Discharge (DoD), Battery Voltage (BV), Charge Rate (C_{rate}), State of Charge (SoC), and Self-Discharge Rate (SDR) were the other battery parameters taken into account for the development of this prediction model.

2.2 Box-Jenkins auto regressive moving average (ARMA) model

The ARMA (Auto Regressive Moving Average) model, chosen using the Box-Jenkins technique, is appropriate for predicting the SoC in Li-ion batteries because of its capacity to handle time-series data with substantial autocorrelations. This method detects patterns and trends by collecting temporal correlations in voltage, current, and temperature. The hybrid technique, which combines ARMA and neural networks, takes advantage of ARMA's linear trend capture and the ANN's nonlinear processing to improve SoC forecast accuracy under dynamic conditions.

For time series analysis and forecasting, a popular mathematical framework is the ARMA model. In order to identify and simulate the underlying patterns in a time series, it integrates two essential elements: the Moving Average (MA) and Auto-Regressive (AR) components [30]. The linear link between the time series' current value and its historical values is explained by the AR component. The weighted total of the prior data is represented by a set of autoregressive parameters. The error terms from previous observations and their impact on the present value are captured by the MA component. The weighted total of the previous error terms is represented by a set of MA parameters. The ARMA model was created using the Box-Jenkins technique to forecast the SoC of EV batteries [31]. There are two parts to the ARMA model. The AR component is the first, and the MA component is the second. When combined, they are denoted as ARMA (å, ῦ), where

Table 1 ARMA model decision criteria based on PACRF and ACRF value behavior

Model	ACRF	PACRF
AR (â)	The time series appears to show a gradual deterioration in correlations between observations as the lag grows, according to decreasing projections towards zero and oscillations in coefficients	Following the lag â, the PACRF shows a declining projection. This shows how observations made at various lags are directly related to one another and identifies the particular lag that greatly influences the observation
MA(v̂)	Following the lag v̂, a diminishing projection to zero implies that the time series values exhibit a sharp decline in correlations with far-off historical observations	The current observation gets impacted by the recent past observations, with the lag making a major contribution, as shown by decreasing projections towards zero and oscillations in coefficient â
ARMA (â, v̂)	An ARMA model's ACRF behavior is characterized by a declining projection to zero following the lag v̂. This is a composite effect, encapsulating the rapid decay with far-off prior observations as well as the delayed decay in correlations	Like the AR component, the PACRF emphasizes the combined influence of both components on the current observation by displaying diminishing projections to zero after the lag â

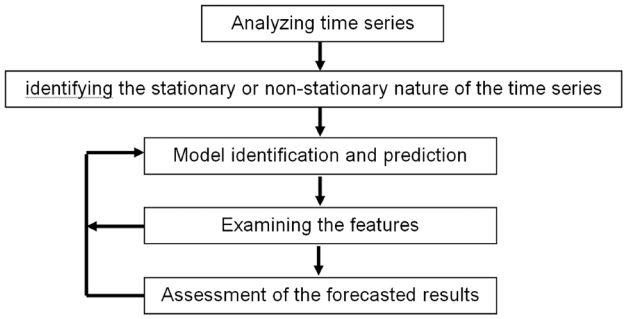

Fig. 1 Procedure of the Box-Jenkins algorithm

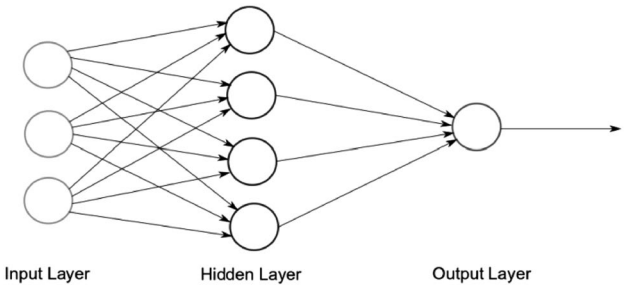

Fig. 2 ANN-based SoC estimation model

ῡ stands for the order of the MA component and å indicates the AR component, respectively. ARMA model's equation is shown in Eq. 4 [32].

$$G_t = \sum_{i=1}^{p} \lambda_i G_{t-1} - \sum_{j=1}^{q} \theta_j ns_{t-j} + ns_t \tag{4}$$

In Eq. 4, G_t is the current value of the time series at time t, $\lambda_i$is the coefficient for the auto-regressive (AR) component, where p is the order of the AR part, G_{t-i} is the value of the time series at previous time step t-I, θ_j is the coefficients for the MA component, q is the order of the MA part, ns_{t-j} is the noise or error term at previous time step t-j and ns_t is the current noise or error term at time t. This equation reflects the dynamics of the time series, capturing both its historical values and the impact of previous errors.

A systematic three-step methodology was used to formulate the ARMA model, with the first stage concentrating on finding the best fit for the time series data. Important statistical tools, such as the Partial Auto-Correlation Function (PACRF) and Auto-Correlation Function (ACRF), were used to accomplish this. The time series' stationary nature was mostly determined by the ACRF, which calculates the correlation between a time series and its lag values. In particular, a sharp decline and flattening of ACRF values suggested a stationary time series with stable underlying patterns.

On the other hand, non-stationary time series showed ACRF values that showed persistent correlations and did not flatten off rapidly. This evaluation, which was based on pattern fluctuations in ACRF values, gave important insights into the time series' temporal dynamics and helped choose a suitable ARMA model for efficient modeling and forecasting. Furthermore, by detecting major contributors to the present observation and capturing direct correlations between observations at various delays, the Partial Auto-Correlation Function (PACRF) enhanced the study. When combined, these resources improved knowledge of time series behavior and helped model developers make well-informed choices [33]. Table 1 indicates the ARMA model selection based on the behavior of the PACRF and ACRF values.

The model is identified as the end of the Box-Jenkins method's first phase. After that, the model's requirements are refined in the second stage, which comprises of parameter estimation. Verification, the third and last phase, is essential to guaranteeing the accuracy of the estimated model. The Ljung-Box test is a commonly employed method during

the verification phase. This statistical technique evaluates if the model's output contains residual autocorrelations. The Ljung-Box test's null hypothesis states that, up to a given lag, there are no residual autocorrelations. Stated differently, it determines whether the model's residuals are independent throughout a range of lag times. To ascertain whether the null hypothesis may be rejected, the test statistic from the Ljung-Box test is compared to crucial values from the ψ^2 distribution [34].

The following is the Ljung-Box equation for determining insignificant residual autocorrelations [34]:

$$LBE = n(n+2)\sum_{k=1}^{h}\frac{\psi_k^2}{n-k} \tag{5}$$

In the above Eq. 5, k is the number of lags, n represents the number of observations in time series, ψ_k is the sample correlation at lag k and h is the maximum lags for consideration in the test. When the value of LBE exceeds 95% of the ψ^2 values, the hypothesis is rejected using the degree of freedom (f) of the ψ^2. Figure 1 indicates the order of actions in Box Jenkins.

2.3 Non-linear auto-regressive network (NLARNN) with feedback based ANN model

The ANN is a sophisticated and essential technique for response prediction in complex, nonlinear systems. ANN is a potent tool for managing complex data interactions because, in contrast to traditional models, it can use intelligent, human-like decision-making processes without being limited by biased assumptions [35]. The core components of ANN models are neural networks, which are made up of hidden layers that intricately connect inputs and outputs, input layers that receive raw data and output layers that offer processed results.

Because of their flexibility and ability to learn from data, ANNs are very much sought for. They can identify intricate patterns and relationships that could pose challenges to traditional models. Figure 2 shows a schematic illustration of an ANN model specifically designed for e-vehicle SoC estimation. ANN can manage non-linearities, adjust to changing conditions, and produce accurate forecasts for crucial parameters like SoC. Because of their adaptability and versatility, ANNs are widely used in a variety of industries. They are especially well-suited for circumstances where the underlying processes are complicated and dynamic. The neural network is an effective tool for forecasting and optimizing important parameters, which eventually improves the performance and efficiency of systems, like e-vehicle batteries, because of its capacity to learn from past data and adjust to new situations [35].

Feedforward backpropagation technique incorporated Multi-Layer Perceptron (MLP) learning network were used in this study. MLP network modeling was chosen because of its excellence in accurately estimating dynamic systems' responses with significantly large precision. This study used a model based on the Non-linear Auto-Regressive Network (NLARNN) with feedback. A particular kind of neural network model used in time series analysis is called NLARNN. It incorporates recurrent neural networks, autoregression, and non-linear behavior. The NLARNN model is capable of recognizing and understanding intricate temporal correlations in sequential data because of its numerous layers and feedback loops. It basically uses the historical values of a time series to forecast future values, which makes it especially useful for activities like signal processing or financial forecasting where it's important to comprehend and forecast sequential patterns. This model depicted a multiple-layer linear autoregressive model with a recurrent network topology throughout. A more accurate estimation was achieved by incorporating previous values from the time series to anticipate subsequent consecutive values. The values of the NLARNN model were determined using the following formula [36].

$$P_t = (P_{t-1} + P_{t-2} + \_\_\_\_\_ + P_{t-d} \tag{6}$$

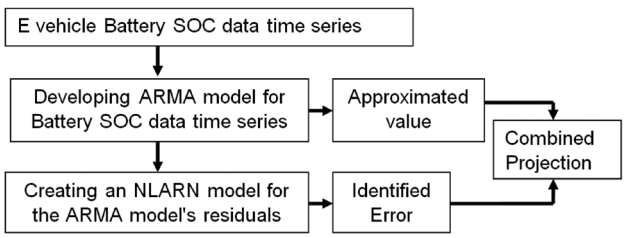

Fig. 3 Integrated hybrid model's pattern

In Eq. 6, P_t is the predicted value at time *t*, P_{t-1}, P_{t-2}..... are the past observed values of the time series. Each P_{t-k} corresponds to the value at time $t-k$, where *k* ranges from 1 to *d*. The lag *d* indicates how many previous values are included in the prediction. Weights were adjusted and the NLARNN model trained using the Levenberg Marquardt (LM) algorithm [37]. For nonlinear (NL) least squares models, LM is a popular optimization technique. In NL regression analysis, it's used to reduce the discrepancy between actual and model-predicted values. The Gauss–Newton method and the technique of steepest descent are both combined in the LM algorithm. The regularization term in the LM algorithm, in contrast to the Gauss–Newton approach, keeps the method from diverging when it comes into contact with noisy data or misrepresented data. During the optimization phase, the algorithm dynamically modifies a parameter that governs this regularization term. LM finds extensive use in many domains, such as scientific research, machine learning, and optimization situations where determining the most suitable variables for a nonlinear model is critical.

2.4 Hybrid model combining Box-Jenkins auto regressive moving average (ARMA) model & non-linear auto-regressive network (NLARNN) with feedback based ANN model

In order to improve prediction and estimation precision, a new strategy that included linear and non-linear systems was utilized. For the purpose of this study, linear information was captured using the developed ARMA model, while non-linear information was collected using the prepared ANN model. Vakili et al. (2017) introduced and developed a combination using these models. Schematic representation of the integrated hybrid model's pattern is shown in Fig. 3.The following equation indicates the construction of this combined model [38]

$$Org_t = C_{Lt} + C_{NLt} \tag{7}$$

In the above Eq. 7, the original sequence of time is indicated as Org_t, the linear component is indicated as C_{Lt} and the nonlinear component is indicated as C_{NLt}. ARMA was used in the first step to represent the core drill rig process variables' linear characteristics. The residuals contained the non-linear characteristics. The residuals ($Resi_t$) were calculated using the following equation based on a linear fit.

$$Resi_t = y_t - \lfloor V_{EST} \rfloor_t \tag{8}$$

In the above Eq. 8, the predicted value of ARMA is indicated as $\lceil VEST \rceil_t$ i and yt is the measurement of the variable at t. Further, Non-linear Auto-Regressive Network (NLARNN) approach was used to model the ARMA model's residuals. The following equation illustrates how the model is expressed using NLARNN.

$$Resi_t = f(Resi_{t-1}, Resi_{t-2}, \ldots \ldots .Resi_{t-d} + Z_t \tag{9}$$

In the above Eq. 9, the non linear function is shown as f and random error is shown as Z_t. The equation of combined hybrid ($Combined_t$) model developed for integrating the linear and non-linear components is shown in Eq. 10

$$\left|Combined_t\right| = \lfloor V_{EST} \rfloor_t + CNL_t \tag{10}$$

2.5 Assessing the hybrid model's performance

The proposed model's accuracy was assessed by utilizing a range of statistical indicators. These performance metrics are essential for evaluating how well the model captures and depicts the underlying patterns in the data. Key statistical metrics that were used were as follows:

1. Coefficient of Determination (R^2): Based on the independent variables, this indicator determines the percentage of the dependent variable's variance that can be predicted. A model that fits the data better is indicated by a higher R^2 score.

$$R_2 = 1 - \frac{\sum \left(y_i - y\prime_i\right)^2}{\sum \left(y_i - y\prime\prime_i\right)^2} \tag{11}$$

In the above Eq. 11, y_i is the actual value, y'_i is the predicted value and y''_i represents the mean of actual values.

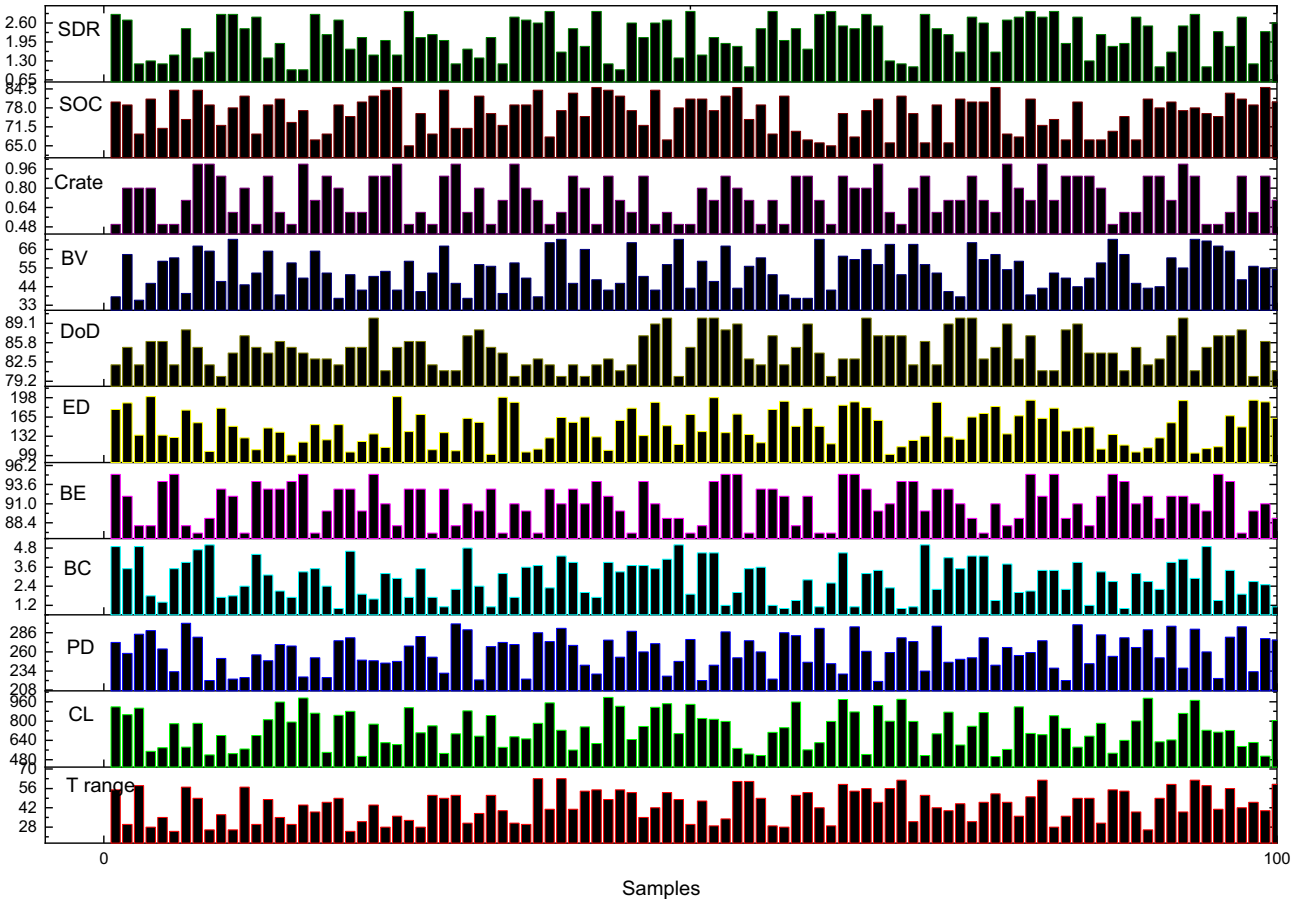

Fig. 4 Data collected for the investigation

2. Mean Bias Error (MBE): The average disparity among the expected and observed values is measured by the Mean Bias Error (MBE). A low MBE indicates that the model's predictions are made impartially.

$$MBE = \frac{1}{n}\sum_{i=1}^{n}\left(y_i - y\prime_i\right) \tag{12}$$

In Eq. 12, n represents the number of data points.

3. Normalized MBE (n-MBE): This normalized type of MBE allows comparisons between different sets of data or models by offering a relative estimate of bias.

$$n - MBE = \frac{MBE}{\overline{y\prime\prime}} \times 100 \tag{13}$$

4. Root Mean Square Error (RMSE): The root mean square error (RMSE) of the average squared discrepancies between the observed and anticipated values is represented. It offers a general indicator of the prediction accuracy of the model.

$$RMSE = \sqrt{\frac{1}{n}\sum_{i=1}^{n}\left(y_i - y\prime_i\right)^2} \tag{14}$$

5. Normalized Root Mean Square Error (n-RMSE): Like n-MBE, n-RMSE normalises the RMSE so that models applied to various datasets can be examined.

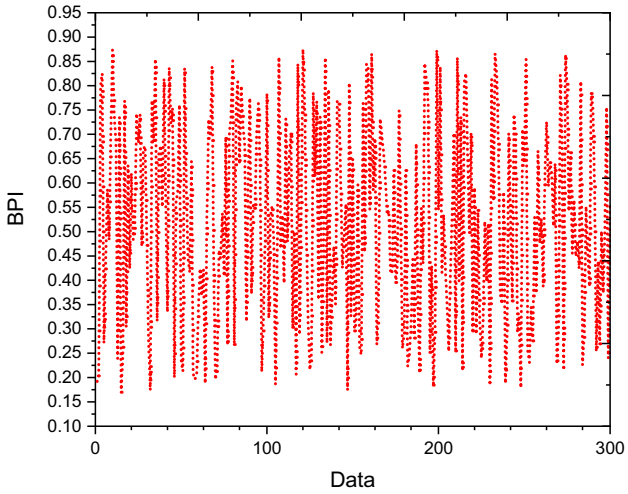

Fig. 5 Fluctuations in the BPI time series

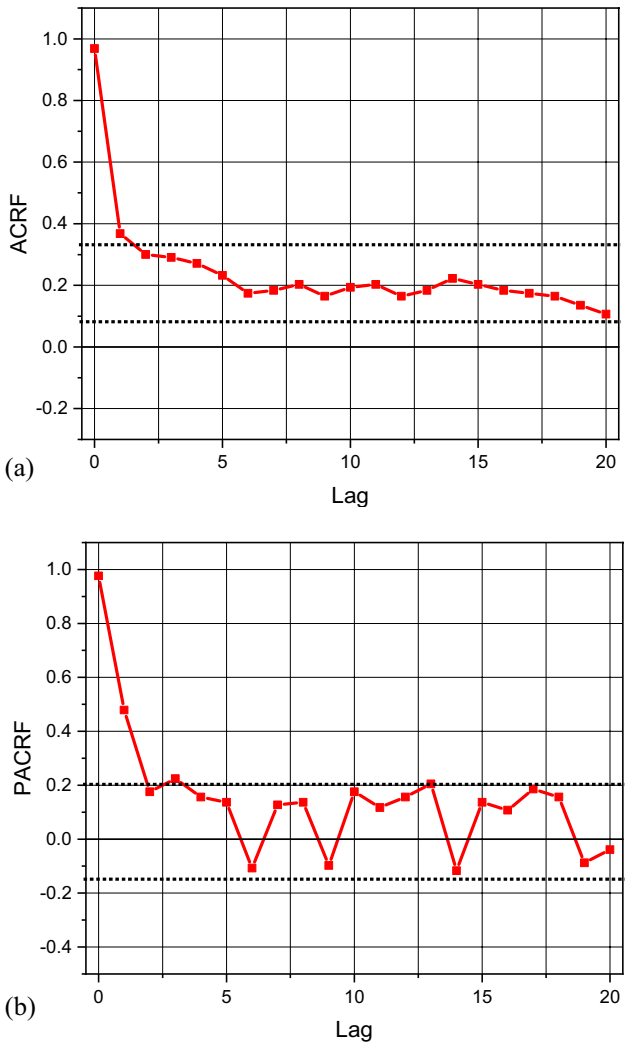

Fig. 6 BPI time series fluctuations for (**a**) ACRF and (**b**) PACRF

$$n - RMSE = \frac{RMSE}{\overline{y''}} \times 100 \tag{15}$$

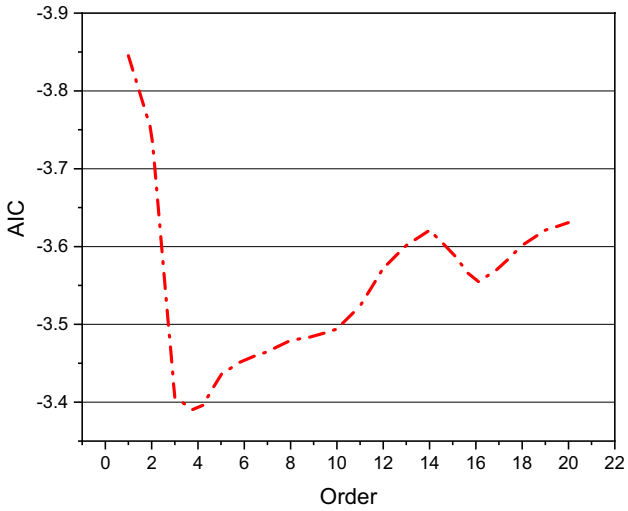

Fig. 7 The values of the AIC based on various model types

Table 2 Features & accuracy indicators of the ARMA (4,0) model

Parameter	p-value	t-Static	Standard error	Estimate
Model 1	0.0836	6.98	0.0407	0.2989
Model 2	0.0721	4.83	0.0384	0.1372
Model 3	0.0369	2.34	0.0377	0.0679
Model 4	0.0107	1.79	0.0319	0.0594

Mean Average Percentage Error (MAPE): The average amount of disparity between the expected and observed values is determined using MAPE. It is especially helpful for comprehending prediction accuracy expressed as a percentage of errors [39].

$$MAPE = \frac{1}{n}\sum_{i=1}^{n}\left|\frac{y_i - y\prime_i}{y_i}\right| \times 100 \tag{16}$$

When taken as a whole, these metrics provide a thorough evaluation of the model's performance, taking into account factors including bias, variability, and overall predicted accuracy. A thorough examination of these indicators facilitates decision-making regarding the produced model's applicability and dependability for a certain application.

3 Results and discussions

3.1 Estimation and prediction of SoC using Box-Jenkins ANN hybrid model

For e-vehicle batteries, the data collected for the important parameters such as working Temperature range (T_{range}), Cycle life (CL), Power Density (PD), Battery Capacity (BC), Battery Efficiency (BE), Energy Density (ED), Depth of Discharge (DoD), Battery Voltage (BV), Charge rate (C_{rate}), SoC & Self Discharge Rate (SDR) are shown in Fig. 4.

The time series must be stationary to be able to use the ARMA model. Yet there was non-stationarity in the data collected regarding the SoC of batteries used in electric vehicles. The Battery Performance Index (BPI) ratio was created to address this issue by comparing Absolute Battery Performance (ABP) to SoC. This method was selected as ABP possessed the ability to determine the battery's true performance. The time series was turned into a stationary form and made more ARMA model-friendly by using the ABP to SoC ratio. By acting as a normalization factor, the

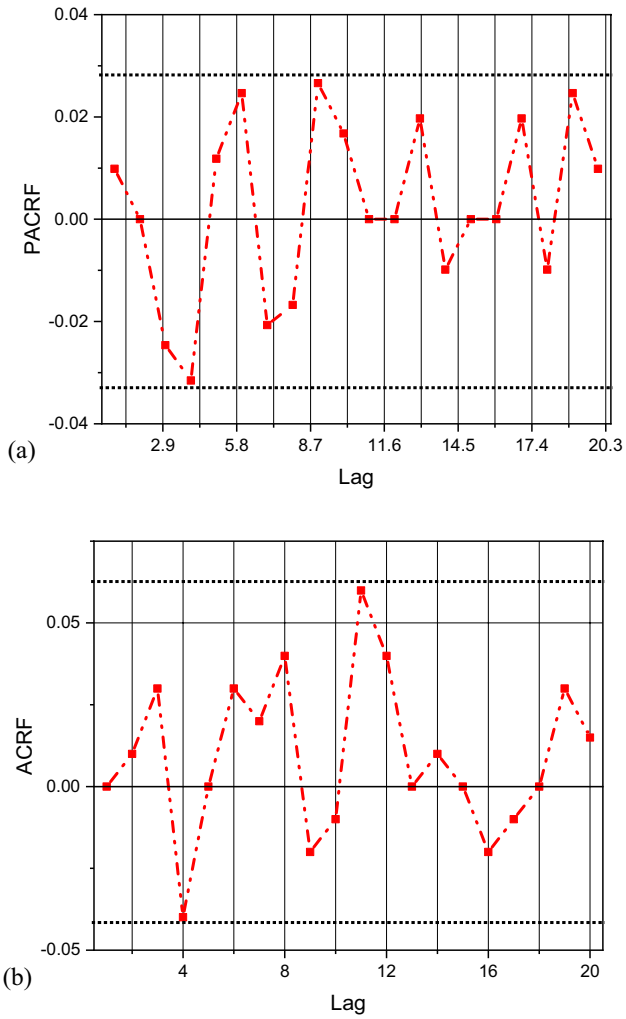

Fig. 8 **a** PACRF, **b** AACRF plots for the ARMA (4, 0) residuals

Battery Performance Index makes it easier to retrieve pertinent information from the non-stationary SoC data. The following is the equation that indicates how the BPI ratio is calculated:

$$\mathrm{BPI} = \frac{\mathrm{ABP}}{\mathrm{SOC}} \tag{17}$$

By reducing non-stationarity by using the Battery Performance Index, this modification makes sure that the patterns of time series in the SoC data are correctly documented. The following formula is used to evaluate ABP.

Table 3 Results of the ARMA (4, 0) model's Ljung-box test

Parameter	Lag (k)			
	12	24	36	48
Chi square	19.39	36.82	53.17	71.29
Q-static	9.62	26.83	38.29	42.84
Degree of Freedom	10	20	32	46
p-value	0.583	0.269	0.293	0.52

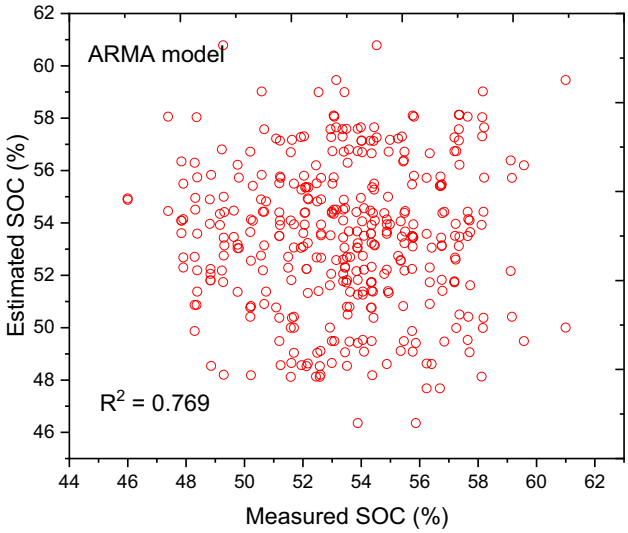

Fig. 9 Relationship between the predicted and observed SoC as determined by the ARMA (4, 0) model

$$ABP = \frac{BQI \times BP_{nom} \times BP_{Act}}{BP_{max}} \quad (18)$$

The Battery Quality Index (BQI), Nominal Battery Performance (BPnom), Actual Battery Performance (BPAct), and Maximum Battery Performance (BPmax) are the terms used in Eq. 18. In Fig. 5, the BPI variances are displayed. Figure 6a and b displays the equivalent ACRF and PACRF, which were plotted for BPI.

After closely examining the ACF plots, which are shown in Fig. 6a, it was found that the curve showed a decreasing tendency after the initial lag. The time series data appear to be stationary based on this drop in the ACF plot. After a few lags, the curve decreased as shown by a study of the Partial Autocorrelation Function (PACF) plots, as shown in Fig. 6b. Variations were considered significant at a 95% confidence level. Following a critical criterion becomes necessary to guarantee the stationarity of the AR factor in the time series. This requirement states that the non-zero values inside the PACF must match the AR model's order. If this requirement is not met, then choosing a higher level for the AR model is preferred. It is imperative to acknowledge that, in the context of the Box-Jenkins methodology, establishing the model order exclusively through PACF variants is inadequate.

As a result, choosing the best order for the AR model depends on the adoption of an appropriate criterion. To determine the best fitting order for the AR model in this situation, the Akaike Information Criterion (AIC) was utilized [40]. The commonly used statistical measure, the AIC, helps choose a frugal but efficient model order by striking a compromise between complexity of the model and goodness of fit. The selection of SoC prediction parameters was based on analyzing ACF and PACF plots. The ACF curve showed a declining trend after the initial lag, indicating stationary time series data. The PACF plots helped determine the AR model's order, ensuring significant variations at

Table 4 Values of the performance indicators for each particular parameter

S No	Parameters	MAPE (%)	RMSE (%)	MBE (%)	R^2 (%)	n-MBE	n-RMSE
1	T_{range}	23.84	32.74	1.69	77.69	0.003.8	0.036
2	CL	34.29	27.52	− 1.27	68.21	− 0.00271	0.031
3	PD	36.82	44.28	1.31	74.25	− 0.00185	0.027
4	BC	41.24	33.78	− 0.83	56.83	− 0.00289	0.046
5	BE	33.42	41.79	2.71	49.71	0.00398	0.059
6	ED	37.52	29.19	1.76	52.41	0.00486	0.073
7	DoD	39.79	33.24	1.49	69.83	0.00418	0.039
8	BV	31.29	34.29	0.69	71.21	0.00246	0.029
9	C_{rate}	29.89	33.41	− 0.34	64.85	− 0.00349	0.042
10	SoC	37.45	29.74	2.41	53.69	0.00281	0.074
11	SDR	33.84	33.74	1.89	57.83	0.00359	0.052

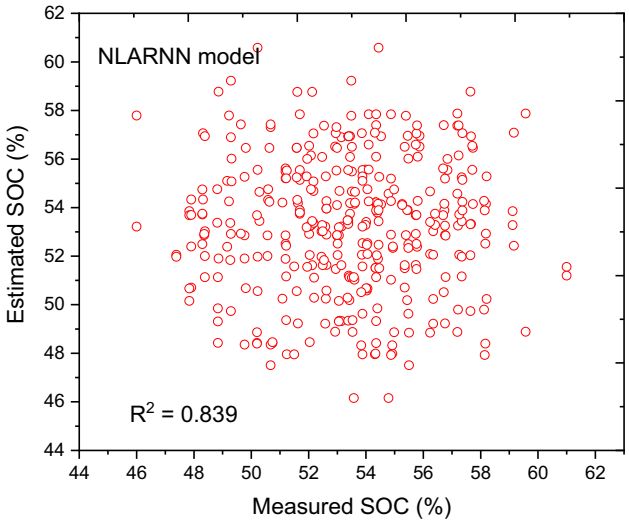

Fig. 10 Observed and predicted SoC correlation based on the NLARNN model

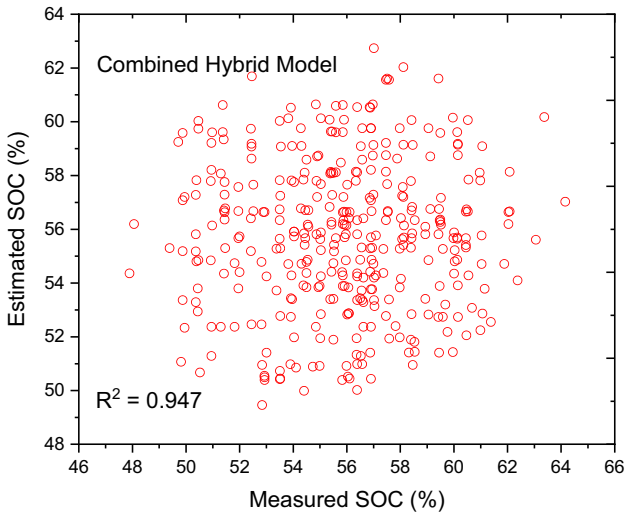

Fig. 11 Relationship between the estimated and measured SoC based on the combined hybrid model

a 95% confidence level. To choose the best model, the Akaike Information Criterion (AIC) was used, balancing model complexity and goodness of fit. Based on the analysis, ARMA (4,0) was selected as the optimal model, demonstrating effective parameter selection for accurate SoC prediction. AIC was calculated according to the below given formula

$$\mathrm{AIC} = \log(k) + \frac{2m}{N} \tag{19}$$

In Eq. 19, log(k) indicates how the model fits with the observed data with the likelihood function k, m is the number of estimated parameters in the model, N is the number of data points, 2 m/N is the penalizing function.

To find the best setup, a number of ARMA models, referred to as ARMA (å, ṽ), were carefully evaluated. A thorough analysis is shown in Fig. 7, where it is found that the Akaike Information Criterion (AIC) value reached its minimum at an order of 4, indicating a satisfactory trade-off among model complexity and goodness of fit. The AIC value increased as the model order was increased further. Thus, in order to evaluate the performance of the core drill rig, ARMA (4, 0) was shown to be the most optimal model.

Table 5 Values of accuracy indicators for the three models

S No	Models	MAPE (%)	RMSE (%)	n-RMSE	R^2 (%)	MBE (%)	n-MBE
1	Single—ARMA	19.742	28.367	0.196	0.769	1.48	0.0032
2	Single—NLARNN	13.789	23.415	0.173	0.839	1.29	0.0027
3	Combined (ARMA + NLARNN) Hybrid	8.363	18.741	0.142	0.947	0.83	0.0016

The relevant parameters of the chosen ARMA (4, 0) model are explained in Table 2, along with the statistical importance of each parameter. These parameters, which are essential for understanding the model's dependability and effectiveness in capturing EV battery SoC, are the p-value, Estimation, the standard Error, and t-Statistic.

The residues must be put through diagnostic testing in order to see whether the selected model is adequate for matching the data series before moving on to model choice and estimation of parameters. Diagnostic tests are essential for verifying if the residuals match the presumptive features of the model. During the diagnostic testing procedure, a careful inspection was carried out to confirm whether the residuals of the chosen ARMA (4, 0) model were independent and conformed to a normal distribution. Establishing that the model correctly represents the basic trends in the data depends on this verification. The PACRF and ACRF distributions of the residuals from the ARMA (4, 0) model are shown in Fig. 8a and b, respectively. These plots contribute to a complete understanding of the model's suitability in reflecting the complexities of the data series by acting as visual aids in evaluating the residuals' independence and normal distribution.

After a thorough analysis of the peaks that were visible in the PACRF plots (Fig. 8a) and (ACRF) plots (Fig. 8b) of the ARMA (4, 0) residuals, it was concluded that these peaks were within the upper and lower 95% confidence levels. After careful examination, it was determined that there was no association between the residuals, proving the prediction errors of the model were independent within the given confidence interval.

The results of the Ljung-Box evaluation of the ARMA (4, 0) model are shown in Table 3, which serves as additional evidence for the independence of residuals. One important finding from the table was that the "p-value" for each lag was more than 0.05 and the calculated Q-statistic was consistently less than the corresponding χ^2 value for all lags. These findings show that there was no association between the residuals and that the Ljung-Box test was considered statistically insignificant. The residuals' clear similarity to unpredictable noise supported the effectiveness of the model. To offer a visual representation of the model's performance, a scatter plot illustrating the relationship between the observed and estimated SoC of the e-vehicle batteries is presented in Fig. 9. The correlation factor (R^2) associated with this scatter plot was computed to be 0.769, underscoring the model's capability to capture and explain a significant portion of the variability in the observed SoC values.

To estimate the Battery Performance Index (BPI), a three-layered Non-Linear Auto-Regressive Neural Network (NLARNN) model with a Multi-Layer Perceptron (MLP) was painstakingly constructed. The model was trained robustly thanks to the use of the feedforward backpropagation approach in the learning process. The gathered dataset was divided into two halves: 25% was set aside for thorough testing, and the remaining 75% was used to train the NLARNN model. As shown in Fig. 6b, a careful study of the Partial Autocorrelation Function (PACRF) values was carried out to establish the proper number of input neurons in the MLP. The inclusion of this lag as input to the neurons in the MLP architecture was initiated by the identification of a delay of 4 in the PACRF plots. The NLARNN model's performance was thoroughly assessed by evaluating various process parameters, including Temperature Range (Trange), Cycle Life (CL), Power Density (PD), Battery Capacity (BC), Battery Efficiency (BE), Energy Density (ED), Depth of Discharge (DoD), Battery Voltage (BV), Charge Rate (Crate), SoC, and Self-Discharge Rate (SDR). The ensuing results, illustrated in Table 4, provide details about the predictive capabilities of the NLARNN model for each parameter.

An incremental progressive strategy was used to determine the best set of inputs for SoC prediction. Following several experiments, the NLARNN model's ideal network structure was determined to have four inputs, one hidden layer with four neurons, and one output. The number of nodes and hidden layers in the MLP model were determined by empirical testing and performance evaluation. The configuration process includes modifying these settings to reduce prediction errors while avoiding overfitting. Typically, the number of hidden layers was chosen based on the dataset's complexity, whereas the number of nodes was decided through trial and error, balancing model accuracy and computing efficiency. These inputs included Depth of Discharge (DoD), Battery Voltage (BV), Charge Rate (Crate), and Energy Density (ED). Figure 10's scatter plot shows how the estimated and observed SoC values for the NLARNN model relate to one another. In a comparative analysis with the ARMA (4, 0) model, the NLARNN model exhibited a notable enhancement, as evidenced

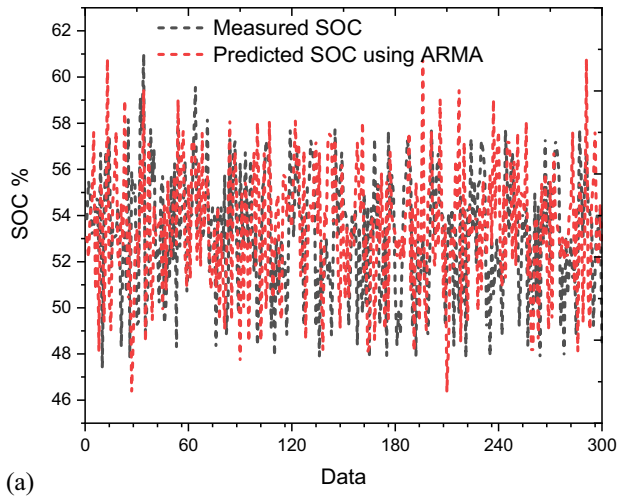

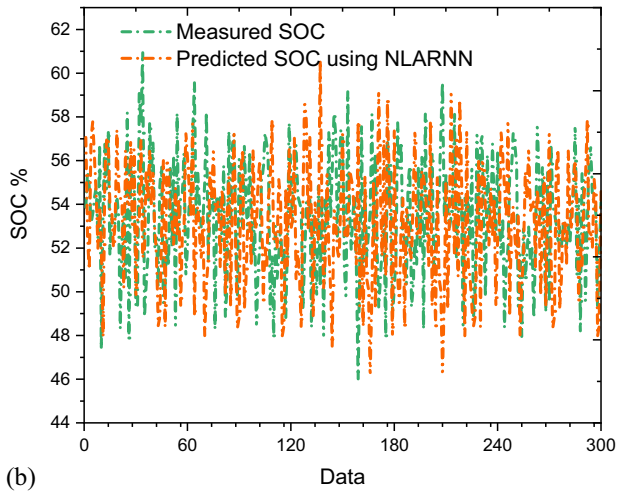

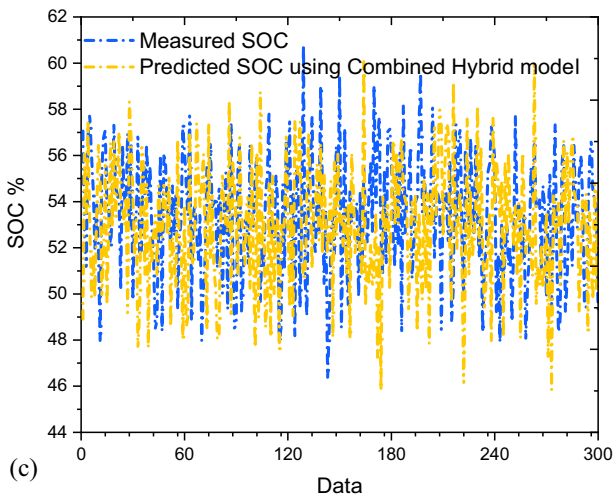

Fig. 12 Plot of the actual SoC values over the SoC values predicted by the (**a**) NLARNN, (**b**) ARMA (4,0), and (**c**) combined hybrid models

Table 6 Comparison of the present study with other works

References	Study	Model used	Advantages	Disadvantages
Ogundana et al., 2024 [41]	Study 1 (NARX ANN)	Nonlinear Autoregressive Neural Network (NARX)	High accuracy in SoC estimation	Complex tuning, higher computational cost
Yang et al., 2023 [42]	Study 2 (SVM)	Support Vector Machine (SVM)	Robust in dynamic conditions, superior to ECM	Requires extensive training data
Bokde et al., 2019 [43]	Study 3 (Hybrid ANN-Kalman)	Hybrid ANN and Kalman Filter	Improves prediction accuracy by compensating for noise	Computationally intensive
Khan et al., 2022 [44]	Study 4 (GA-Grey Model)	Genetic Algorithm optimized Grey Model	Adaptive, good for nonlinear behavior	Relatively lower accuracy in real-time applications
Current Stud	Present Research (Box-Jenkins ANN Hybrid)	Box-Jenkins combined with ANN	Improved R^2 value (0.947), high prediction accuracy, lower errors (MAPE 8.36%)	Slightly complex but significantly enhances accuracy

by an increased R^2 value of 0.839. This improvement underscores the NLARNN model's superiority in capturing the underlying complexities of the Battery Performance Index when compared to the ARMA model.

The residuals from the ARMA model were used as inputs for a new Multi-Layer Perceptron (MLP) model in order to build the integrated hybrid model. This hybrid model was trained using the Levenberg–Marquardt technique. The goal of input normalisation was to improve the model's performance and convergence by keeping it within the range of 0 and 1.

Leveraging the unique strengths of the Non-Linear Auto-Regressive Neural Network (NLARNN) model and the ARMA model was the goal behind developing this combined hybrid model. By utilizing these two models' complementing qualities, the hybridization intended to improve the overall predictive power.

Figure 11 shows the correlations that the combined hybrid model produced between the estimated and observed SoC values. This hybrid model's remarkable R^2 value of 0.947 highlights its resilience and significant improvement over individual models. This high R^2 value highlights the hybrid model's improved prediction performance by showing that it successfully captures a significant amount of the variability in the observed SoC values.

High predictability was demonstrated by the combined hybrid model, which had an R^2 value higher than that of the ARMA and NLARNN models. The hybrid model's improved capacity to explain and capture fluctuations in SoC is indicated by this high R^2 value. The enhanced predictability can be ascribed to the complementary application of the ARMA and NLARNN models, which together augment the dataset's modeling of intricate interactions.

To offer a quantitative evaluation of the prediction accuracy, statistical indicators were employed to determine the expected SoC values from the ARMA, NLARNN, and combined hybrid models, as indicated in Table 5. The comparison revealed a difference between the measured and predicted values, with the NLARNN model generating predictions that were closer to the actual values. Notably, the combined hybrid model demonstrated notably higher prediction accuracies when compared to the ARMA and NLARNN models. The scatter plots in Fig. 12a–c illustrate the relationships between the predicted and measured SoC values for the ARMA, NLARNN, and hybrid models, respectively. The hybrid model as a whole outperforms the individual models, indicating that it can more nearly approximate the real SoC values. Figure 12 showed that the combined hybrid model's precision outperformed the other two models. Comparative analysis of other ANN models are shown in Table 6.

The current study had a high R^2 value of 0.947 compared to previous studies, indicating a better ability to capture SoC fluctuations. The hybrid model dramatically reduced the Mean Absolute Percentage Error (MAPE), providing better accuracy than previous approaches. Furthermore, the combination of the Box-Jenkins and ANN models achieved a balance of complexity and accuracy, beating separate models in overall performance.

4 Conclusions

This study presented a unique method for forecasting the state of charge (SoC) of lithium-ion batteries in electric vehicles by combining a Non-Linear Auto-Regressive Neural Network (NLARNN) model with the Box-Jenkins Auto-Regressive Moving Average (ARMA) model. The innovative application of the Battery Performance Index altered non-stationary data, making the model more applicable. The hybrid model outperformed ARMA (0.769) and NLARNN (0.839), with a R^2 value of 0.947. This demonstrates the efficiency of combining models to increase forecast accuracy, particularly with crucial factors like Charge Rate and Depth of Discharge, which resulted in a mean absolute percentage error reduction of 8.363%.

Acknowledgements The authors would like to acknowledge the assistance provided by R&D, M/s. Vikram Engineering Industry, Tiruchirappalli, India for conducting the experiments related to batteries.

Author contributions Ms. Glarida Amala Louis contributed to manuscript preparation and technical working. Dr. Siddharth Sampathkumar contributed to supervision, proofing, completion and validation of this research work.

Data availability Data is provided within the manuscript.

Declarations

Competing interests The authors declare no competing interests.

References

1. Adedeji BP. Electric vehicles survey and a multifunctional artificial neural network for predicting energy consumption in all-electric vehicles. Results Eng. 2023;19: 101283.
2. Tiwari H, Ghosh A, Sain C, Ahmad F, Al-Fagih L. Modified direct torque control algorithm for regeneration capability of IM driven electric vehicle by using hybrid energy storage system. Renew Energy Focus. 2024:100534.
3. Tan G, Wu F, Zhan C, Wang J, Mu D, Lu J, Amine K. Solid-state li-ion batteries using fast, stable, glassy nanocomposite electrolytes for good safety and long cycle-life. Nano Lett. 2016;16(3):1960–8.
4. Chemali E, Kollmeyer PJ, Preindl M, Emadi A. State-of-charge estimation of Li-ion batteries using deep neural networks: a machine learning approach. J Power Sources. 2018;400:242–55.
5. Manoharan A, Sooriamoorthy D, Begam KM, Aparow VR. Electric vehicle battery pack state of charge estimation using parallel artificial neural networks. J Energy Storage. 2023;72: 108333.
6. Kamali MA, Lim W. ANN-based state of charge estimation of li-ion batteries for embedded applications. Jurnal Nasional Teknik Elektro dan Teknologi Informasi. 2023;12(2):85–92.
7. Nouri A, Lachheb A, El Amraoui L. Optimizing efficiency of Vehicle-to-Grid system with intelligent management and ANN-PSO algorithm for battery electric vehicles. Electr Power Syst Res. 2024. https://doi.org/10.1016/j.epsr.2024.108546.
8. Afzal MZ, Aurangzeb M, Iqbal S. A novel electric vehicle battery management system using an artificial neural network-based adaptive droop control theory. J Energy Storage. 2023. https://doi.org/10.1016/j.est.2023.107563.
9. Adedeji BP, Kabir G. A feedforward deep neural network for predicting the state-of-charge of lithium-ion battery in electric vehicles. Decis Anal J. 2023. https://doi.org/10.1016/j.decan.2023.100295.
10. Mehmandoosti MM, Kowsary F. Artificial neural network-based multi-objective optimization of cooling of lithium-ion batteries used in electric vehicles utilizing pulsating coolant flow. Appl Therm Eng. 2023. https://doi.org/10.1016/j.applthermaleng.2023.127311.
11. Olabi AG, Abdelghafar AA, Soudan B, Alami M. Artificial neural network driven prognosis and estimation of lithium-ion battery states: current insights and future perspectives. Ain Shams Eng J. 2024. https://doi.org/10.1016/j.asej.2024.102342.
12. Çolak AB. A new study on the prediction of the effects of road gradient and coolant flow on electric vehicle battery power electronics components using machine learning. J Energy Storage. 2023. https://doi.org/10.1016/j.est.2023.106153.
13. Kurucan M, Özbaltan M, Yetgin Z, Alkaya A. Applications of artificial neural network based battery management systems: a literature review. Renew Sustain Energy Rev. 2024. https://doi.org/10.1016/j.rser.2024.114473.
14. Naresh VS, Ratnakara Rao GV. Predictive machine learning in optimizing the performance of electric vehicle batteries: techniques, challenges, and solutions. Data Min Knowl Discov Rev. 2024. https://doi.org/10.1002/dmkr.10839.
15. Wei M, Ye M, Zhang C, Lian G, Xia B, Wang Q. Robust state of charge estimation of LiFePO4 batteries based on Sage-Husa adaptive Kalman filter and dynamic neural network. Electrochim Acta. 2024;50:718.
16. Shrivastava P, Naidu PA, Sharma S. Review on technological advancement of lithium-ion battery states estimation methods for electric vehicle applications. J Energy Storage. 2023. https://doi.org/10.1016/j.est.2023.107234.
17. Oyucu S, Doğan F, Aksöz A, Biçer E. Comparative analysis of commonly used machine learning approaches for Li-ion battery performance prediction and management in electric vehicles. Appl Sci. 2024. https://doi.org/10.3390/app14092982.
18. Badran MA, Toha SF. Employment of artificial intelligence (AI) techniques in battery management system (BMS) for electric vehicles (EV): issues and challenges. Pertanika J Sci Technol. 2024. https://doi.org/10.47836/pjst.30.2.09.
19. Hong J, Zhang H, Xu X. Thermal fault prognosis of lithium-ion batteries in real-world electric vehicles using self-attention mechanism networks. Appl Therm Eng. 2023. https://doi.org/10.1016/j.applthermaleng.2023.127476.
20. Scarpelli C, Gazzarri J, Huria T, Lutzemberger G, Ceraolo M. Neural network for the estimation of LFP battery SOH cycled at different power levels. J Energy Storage. 2023;66: 107027.
21. Lipu MSH, Miah MS, Jamal T, Rahman T, Ansari MI. Artificial intelligence approaches for advanced battery management systems in electric vehicle applications: a statistical analysis towards future research opportunities. Vehicles. 2023. https://doi.org/10.3390/vehicles7010002.
22. Wang S, Ren P, Takyi-Aninakwa P, Jin S, Fernandez C. A critical review of improved deep convolutional neural network for multi-timescale state prediction of lithium-ion batteries. Energies. 2022;15(14):5053.
23. Dvorak D, Bäuml T, Holzinger A, Popp H. A comprehensive algorithm for estimating lithium-ion battery parameters from measurements. IEEE Trans Sustain Energy. 2017;9(2):771–9.
24. Redondo-Iglesias E, Venet P, Pelissier S. Global model for self-discharge and capacity fade in lithium-ion batteries based on the generalized Eyring relationship. IEEE Trans Veh Technol. 2017;67(1):104–13.
25. Liu G, Ouyang M, Lu L, Li J, Han X. Analysis of the heat generation of lithium-ion battery during charging and discharging considering different influencing factors. J Therm Anal Calorim. 2014;116:1001–10.
26. Such MC. Operation and control strategies for battery energy storage systems to increase penetration levels of renewable generation on remote microgrids. 2013.
27. Chiang YH, Sean WY, Wu CH, Huang CY. Development of a converterless energy management system for reusing automotive lithium-ion battery applied in smart-grid balancing. J Clean Prod. 2017;156:750–6.

28. Di Domenico D, Fiengo G, Stefanopoulou A. Lithium-ion battery state of charge estimation with a Kalman filter based on an electrochemical model. In: 2008 IEEE International Conference on Control Applications. 2008; pp 702–7. IEEE.
29. Zheng Y, Wu H, Yi W, Lai X, Dai H, Han X, Ouyang M. A novel classification method of commercial lithium-ion battery cells based on fast and economic detection of self-discharge rate. J Power Sources. 2020;478: 229039.
30. Chen Z, Xue Q, Xiao R, Liu Y, Shen J. State of health estimation for lithium-ion batteries based on fusion of autoregressive moving average model and Elman neural network. IEEE Access. 2019;7:102662–78.
31. Kim S, Lee PY, Lee M, Kim J, Na W. Improved State-of-health prediction based on auto-regressive integrated moving average with exogenous variables model in overcoming battery degradation-dependent internal parameter variation. J Energy Storage. 2022;46: 103888.
32. Huang L. Auto regressive moving average (ARMA) modeling method for Gyro random noise using a robust Kalman filter. Sensors. 2015;15(10):25277–86.
33. Valipour M, Banihabib ME, Behbahani SMR. Parameters estimate of autoregressive moving average and autoregressive integrated moving average models and compare their ability for inflow forecasting. J Math Stat. 2012;8(3):330–8.
34. Wenning Z, Valenci E. A Monte Carlo simulation study on the power of autocorrelation tests for ARMA models. Am J Undergrad Res. 2019;16(3):59.
35. Voyant C, Muselli M, Paoli C, Nivet ML. Numerical weather prediction (NWP) and hybrid ARMA/ANN model to predict global radiation. Energy. 2012;39(1):341–55.
36. Cinar AC. Training feed-forward multi-layer perceptron artificial neural networks with a tree-seed algorithm. Arab J Sci Eng. 2020;45(12):10915–38.
37. Lourakis MI. A brief description of the Levenberg-Marquardt algorithm implemented by levmar. Found Res Technol. 2005;4(1):1–6.
38. Vakili M, Sabbagh-Yazdi SR, Khosrojerdi S, Kalhor K. Evaluating the effect of particulate matter pollution on estimation of daily global solar radiation using artificial neural network modeling based on meteorological data. J Clean Prod. 2017;141:1275–85.
39. Arsenović M, Pezo L, Stanković S, Radojević Z. Factor space differentiation of brick clays according to mineral content: prediction of final brick product quality. Appl Clay Sci. 2015;115:108–14.
40. Akaike H. Akaike's information criterion. Int Encycl Stat Sci. 2011;25–5.
41. Ogundana AS, Terala PK, Amarasinghe M, Xiang X, Foo SY. Electric vehicle battery state of charge estimation with an ensemble algorithm using central difference Kalman filter (CDKF) and non-linear autoregressive with exogenous input (NARX). IEEE Access. 2024.
42. Yang D, Yu J, He Z, Li P, Du X. Applying self-powered sensor and support vector machine in load energy consumption modeling and prediction of relational database. Sci Rep. 2023;13(1):19097.
43. Bokde N, Feijóo A, Villanueva D, Kulat K. A review on hybrid empirical mode decomposition models for wind speed and wind power prediction. Energies. 2019;12(2):254.
44. Khan K, Iqbal M, Jalal FE, Amin MN, Alam MW, Bardhan A. Hybrid ANN models for durability of GFRP rebars in alkaline concrete environment using three swarm-based optimization algorithms. Constr Build Mater. 2022;352: 128862.

Terms and Conditions

Springer Nature journal content, brought to you courtesy of Springer Nature Customer Service Center GmbH (“Springer Nature”).
Springer Nature supports a reasonable amount of sharing of research papers by authors, subscribers and authorised users (“Users”), for small-scale personal, non-commercial use provided that all copyright, trade and service marks and other proprietary notices are maintained. By accessing, sharing, receiving or otherwise using the Springer Nature journal content you agree to these terms of use (“Terms”). For these purposes, Springer Nature considers academic use (by researchers and students) to be non-commercial.
These Terms are supplementary and will apply in addition to any applicable website terms and conditions, a relevant site licence or a personal subscription. These Terms will prevail over any conflict or ambiguity with regards to the relevant terms, a site licence or a personal subscription (to the extent of the conflict or ambiguity only). For Creative Commons-licensed articles, the terms of the Creative Commons license used will apply.
We collect and use personal data to provide access to the Springer Nature journal content. We may also use these personal data internally within ResearchGate and Springer Nature and as agreed share it, in an anonymised way, for purposes of tracking, analysis and reporting. We will not otherwise disclose your personal data outside the ResearchGate or the Springer Nature group of companies unless we have your permission as detailed in the Privacy Policy.
While Users may use the Springer Nature journal content for small scale, personal non-commercial use, it is important to note that Users may not:

1. use such content for the purpose of providing other users with access on a regular or large scale basis or as a means to circumvent access control;
2. use such content where to do so would be considered a criminal or statutory offence in any jurisdiction, or gives rise to civil liability, or is otherwise unlawful;
3. falsely or misleadingly imply or suggest endorsement, approval , sponsorship, or association unless explicitly agreed to by Springer Nature in writing;
4. use bots or other automated methods to access the content or redirect messages
5. override any security feature or exclusionary protocol; or
6. share the content in order to create substitute for Springer Nature products or services or a systematic database of Springer Nature journal content.

In line with the restriction against commercial use, Springer Nature does not permit the creation of a product or service that creates revenue, royalties, rent or income from our content or its inclusion as part of a paid for service or for other commercial gain. Springer Nature journal content cannot be used for inter-library loans and librarians may not upload Springer Nature journal content on a large scale into their, or any other, institutional repository.
These terms of use are reviewed regularly and may be amended at any time. Springer Nature is not obligated to publish any information or content on this website and may remove it or features or functionality at our sole discretion, at any time with or without notice. Springer Nature may revoke this licence to you at any time and remove access to any copies of the Springer Nature journal content which have been saved.
To the fullest extent permitted by law, Springer Nature makes no warranties, representations or guarantees to Users, either express or implied with respect to the Springer nature journal content and all parties disclaim and waive any implied warranties or warranties imposed by law, including merchantability or fitness for any particular purpose.
Please note that these rights do not automatically extend to content, data or other material published by Springer Nature that may be licensed from third parties.
If you would like to use or distribute our Springer Nature journal content to a wider audience or on a regular basis or in any other manner not expressly permitted by these Terms, please contact Springer Nature at

onlineservice@springernature.com